Systems & Control Transactions

Research Article
Foundations of Computer Aided Process Design (FOCAPD 2024)
Breckenridge, Colorado, USA. July 14-18, 2024
Peer Reviewed Conference Proceeding

PSE PRESS

Equation-Oriented Modeling of Water-Gas Shift Membrane Reactor for Blue Hydrogen Production

Damian T. Agi[a], Hani A. E. Hawa[b], and Alexander W. Dowling[a]*

[a] University of Notre Dame, Department of Chemical and Biomolecular Engineering, South Bend, IN, United States
[b] Precision Combustion, Inc., North Haven, CT, United States
* Corresponding Author: adowling@nd.edu.

ABSTRACT

Water-gas shift membrane reactors (WGS-MRs) offer a pathway to affordable blue H_2 generation/purification from gasified feedstock or reformed fuels. To exploit their cost benefits for blue hydrogen production, WGS-MRs' performance needs to be optimized, which includes navigating the multidimensional design space (e.g., temperature, feed pressures, space velocity, membrane permeance and selectivity, catalytic performance). This work describes an equation-oriented modeling framework for WGS-MRs in the Pyomo ecosystem, with an emphasis on model scaling and multi-start initialization strategies to facilitate reliable convergence with nonlinear optimization solvers. We demonstrate, through sensitivity analysis, that our model converges rapidly (< 1 CPU second on a laptop computer) under a wide range of operating parameters (e.g., feed pressures of 1-3 MPa, reactor temperatures of 624-824 K, sweep-to-feed ratios of 0-0.5, and steam/carbon ratios of 1-5). Ongoing work includes (1) validation and calibration of the WGS-MR model using benchtop laboratory data and (2) design, intensification, and optimization of blue H_2 processes using the WGS-MR model.

Keywords: Modelling, Membranes, Hydrogen, Process Design, Water-Gas Shift, Model Initialization

INTRODUCTION

The water-gas shift (WGS) reaction is essential for converting CO into CO_2 and producing additional hydrogen from syngas generated from reforming or gasification [1-2]. WGS is especially critical in blue H_2 production technologies, where the produced CO_2 is captured and sequestrated downstream [3].

WGS is an established industrial reaction that has been broadly studied [4]. Ebrahimi et al. [5] provide a comprehensive overview of the WGS reaction, including the CO conversion, H_2 selectivity, and structural properties of transition and noble metal catalysts on oxide and carbon-based supports. The state-of-the-art design for WGS reactors includes a two-staged packed bed reactor: a high-temperature shift (643 K to 673 K) stage followed by inter-stage cooling and then a low-temperature shift (450 K to 553 K) [6]. One prevailing challenge with WGS is that it is a reversible and exothermic reaction ($\Delta H^0_{298} = -41$ kJ/mol), which imposes thermodynamic limitations on the attainable conversion.

Incorporating a membrane within a water gas shift reactor enhances H_2 production [2, 6-7]. H_2-selective membranes (e.g., dense metallic membranes, polymer membranes, and other inorganic membranes) have been previously used for this purpose [7-8]. Particularly, Pd-based membranes are promising for H_2 separation due to their ultra-high H_2-selectivity [2, 9]. One major challenge with Pd-based membranes is inadequate thermal stability/chemical tolerance in these harsh operating conditions, which can be mitigated by alloying Pd with other elements [2, 10]. Pd-based membranes are used for H_2 production in the form of membrane separators [7, 10] or membrane reactors, i.e., membrane reformers or water-gas shift membrane reactors (WGS-MR) [9, 11].

WGS-MRs offer the added benefit of combining separation and reaction in one unit, providing process intensification opportunities. The continuous separation of H_2 from the reactor through Pd-based membranes provides three distinct advantages:

1. The thermodynamic equilibrium continuously shifts in favor of the forward reaction, leading to

improved CO conversion [2, 12, 13].

2. The continuous production of H_2 from the reaction boosts the H_2 partial pressure on the retentate side, enhancing the recovery of H_2 through separation.
3. The retentate is a high-pressure CO_2-concentrated stream, making carbon capture less energy intensive [14].

Mathematical modeling and numerical simulation are needed to elucidate the design of WGS-MRs for maximizing technical and economic benefits [7, 9, 12]. Membrane modules have been widely modeled in flow sheet simulators such as Aspen Plus to support process-scale optimization and technoeconomic analysis [13, 15]. Our approach, based on equation-oriented (EO) design, supports the simultaneous solution of the various model equations, making it easier to embed them directly into large-scale optimization models [16-18]. However, EO models require careful equation and variable scaling and initialization to ensure reliable solver convergence [19]. Additionally, the literature on EO modeling of WGS-MR is notably sparse, with significant contributions from Gosieswki et al. [14].

This brief paper introduces an EO modeling framework of WGS-MRs. We focus on model scaling analysis and multi-start initialization strategies to promote fast and reliable convergence in the solution of the nonlinear model. Finally, we show the model's capabilities for the rapid study of the WGS-MR system through sensitivity analysis.

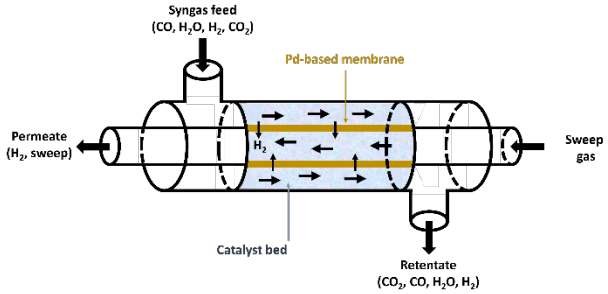

Figure 1. Schematic of a WGS-MR module. The syngas feed flows on the shell side, which is packed with a catalyst for the WGS reaction; the tube is made of a Pd-based membrane that is selectively permeable to H_2; permeated H_2 and an optional sweep gas flow on the tube side in a counter-current flow direction. Based on similar schematics in Brunetti et al. [9].

METHODS

WGS-MR model

We consider a cylindrical, tube-in-shell reactor module with the reaction occurring on the shell side in a packed catalyst bed, as shown in **Figure 1**. The tube comprises a Pd-based membrane that selectively supports H_2 permeation, which flows on the tube side in a counter-current direction.

Mass Balance:

The retentate side mass balance for this reactor configuration is given as:

$$\frac{dF_{ret,i}}{dz} = -J_i \frac{A_{mem}}{l} + \nu_i(-r_{CO})\frac{V_{rxn}}{l}. \quad (1)$$

Similarly, the permeate side mass balance is given as:

$$\frac{dF_{perm,i}}{dz} = -J_i \frac{A_{mem}}{l}, \quad (2)$$

where $F_{ret,i}$ (mol s^{-1}) and $F_{perm,i}$ (mol s^{-1}) are the retentate and permeate side flowrates of species i respectively; z (m) is the axial distance along the WGS-MR module; A_{mem} (m^2) is the membrane area; l (m) is the total length of the module; ν_i (unitless) is the stoichiometric coefficient of species i in the WGS reaction; r_{CO} (mol m^{-3} s^{-1}) is the reaction rate of CO in the WGS reaction; V_{rxn} (m^3) is the retentate side volume of the WGS-MR available for the reaction. J_i (mol m^{-2} s^{-1}) is the flux of species i through the Pd-based membrane.

The flux, J_i is defined by the Sievert-type expression [9, 20]:

$$J_i = \begin{cases} Q(T)\left[\left(P_{ret}y_{ret,i}+\varepsilon\right)^n - \left(P_{perm}y_{perm,i}+\varepsilon\right)^n\right], & i = H_2 \\ 0, \text{ otherwise} \end{cases} \quad (3)$$

Here, $Q(T)$ (mol m^{-2} Pa$^{-0.5}$ s^{-1}) is the permeance of the membrane, which correlates with the reactor temperature as given in **Eq. (4)**. P_{ret} (Pa) and P_{perm} (Pa) are the retentate and permeate side pressures, respectively. $y_{ret,i}$ and $y_{perm,i}$ are the retentate and permeate side compositions of gas species i, respectively, as defined in **Eq. (5)**. The Sievert's law pressure exponent, n, ranges from 0 to 1 and takes a value of 0.5 for the ideal Sievert behavior where the diffusion of H atoms in the bulk Pd metal forms the rate-limiting step for H_2 permeation in the Pd-based membrane, and the Pd-H system is infinitely diluted [20]. ε is a small number (e.g., 10^{-8}) that prevents computing the $n < 1$ exponent of near zero when the partial pressure is very small.

$$Q(T) = Q_0 exp\left(-\frac{E_a}{RT}\right), \quad (4)$$

$$y_{ret,i} = \frac{F_{ret,i}}{\sum_j F_{ret,j}}, \quad y_{perm,i} = \frac{F_{perm,i}}{\sum_j F_{perm,j}}. \quad (5)$$

In **Eq. (4)**, Q_0 (mol m^{-2} Pa$^{-0.5}$ s^{-1}) is the pre-exponential factor; E_a (J mol^{-1}) is the activation energy of permeation; and R is the universal gas constant (8.314 J mol^{-1} K^{-1}).

WGS is a reversible exothermic reaction given in **Eq. (6)** [9]. In this work, we use the reaction rate expression, **Eq. (7)**, proposed by Amadeo and Laborde [21] for WGS catalyzed by copper/zinc oxide/alumina.

$$CO + H_2O \rightleftharpoons H_2 + CO_2 \quad \Delta H^0_{298K} = -41\ \text{kJ/mol} \tag{6}$$

$$-r_{CO} = \frac{0.92\, e^{\left(-\frac{454.3}{T}\right)} P_{CO} P_{H2O}\left(1-\left(\frac{P_{CO2}P_{H2}}{P_{CO}P_{H2O}}\right)\left(\frac{1}{K_{eq}}\right)\right)}{\left(1+2.2\, e^{\left(\frac{101.5}{T}\right)} P_{CO}+0.4\, e^{\left(\frac{158.3}{T}\right)} P_{H2O}+0.0047\, e^{\left(\frac{2737.9}{T}\right)} P_{CO2}+0.05\, e^{\left(\frac{1596.1}{T}\right)} P_{H2}\right)^2} \times 16.6667\, \rho_{catalyst}, \tag{7}$$

where P_{CO}, P_{H2O}, P_{CO2}, and P_{H2} denote the partial pressures in Pa of gas species, CO, H_2O, CO_2, and H_2, respectively, $\rho_{catalyst}$ (kg m^{-3}) is the density of the WGS catalyst, and T (K) is the reactor temperature. The 16.6667 multiplier enforces unit conversion from mol g^{-1} min^{-1} to mol kg^{-1} s^{-1} units. K_{eq} is the equilibrium constant, given by [22]:

$$K_{eq} = 1.2 \times 10^{-2}\, e^{\left(\frac{4639}{T}\right)}. \tag{8}$$

Momentum Balance:

Assuming constant pressure drop on both sides of the Pd-based membrane, the momentum balances in the WGS-MR are as follows:

$$\frac{dP_{ret}}{dz} = \text{constant}, \quad \frac{dP_{perm}}{dz} = \text{constant}. \tag{9}$$

A total pressure drop of 35 kPa was used on the retentate side and 0 kPa on the permeate side.

The boundary conditions for the WGS-MR module are:

$$z = 0: F_{ret,i} = y_{feed,i} F_0, \quad P_{ret} = P_{feed}, \tag{10}$$

$$z = l: F_{perm,i} = y_{sweep,i} F_{sweep}, \quad P_{perm} = P_{sweep}, \tag{11}$$

where F_0 (mol s^{-1}) is the total feed flowrate and F_{sweep} (mol s^{-1}) is the total sweep flowrate.

Model scaling

The material balances in **Eqs. (1)** & **(2)** result in poor solver convergence when the component flowrates, J_i, are near minimal values ($\leq 10^{-4}$). To circumvent this, we apply dimensionless analysis to scale the flowrates and axial distance using the characteristic parameters F_0 and l:

$$\bar{F} = \frac{F}{F_0} \leftrightarrow dF = F_0 d\bar{F} \tag{12}$$

$$\bar{z} = \frac{z}{l} \leftrightarrow dz = l d\bar{z}\,. \tag{13}$$

The material balances in **Eqs. (1)** & **(2)** become:

$$\frac{d\bar{F}_{ret,i}}{d\bar{z}} = -J_i \frac{A_{mem}}{F_0} + \nu_i(-r_{CO}) \frac{V_{rxn}}{F_0} \tag{14}$$

$$\frac{d\bar{F}_{perm,i}}{d\bar{z}} = -J_i \frac{A_{mem}}{F_0} \tag{15}$$

The boundary conditions in **Eqs. (10)** and **(11)** are updated accordingly by dividing the component flowrates ($y_{feed,i}F_0$ and $y_{sweep,i}F_{sweep}$) by F_0.

Table 1 reports the model parameters used in this study.

Table 1. WGS-MR model parameters. These parameters are based on the work of Brunetti et al. [9]. *Estimated from property data.

Parameter	Value	Description
A_{mem} (m^2)	1.57×10^{-2}	Membrane area
V_{rxn} (m^3)	3.93×10^{-5}	Reaction volume
Q_0 (mol m^{-2} s^{-1} Pa$^{-0.5}$)	1.62×10^{-2}	Permeance pre-exponential factor
$\frac{E_a}{R}$ (K)	3.10×10^3	Activation energy of permeation per gas constant
$\rho_{catalyst}$ (kg m^{-3})	1.38×10^3	Catalyst density
n (unitless)	0.5	H_2 partial pressure exponent
F_0 (mol s^{-1})	$1.26 \times 10^{-3*}$	Feed flowrate
T (K)	553	Reactor temperature
P_{feed} (MPa)	1	Feed pressure
P_{sweep} (MPa)	0.1	Sweep-side pressure
$y_{feed,CO}$ (vol%)	20	Molar composition of gas species in the feed
$y_{feed,H2O}$ (vol%)	20	
$y_{feed,CO2}$ (vol%)	10	
$y_{feed,H2}$ (vol%)	50	

Numerical solution and computational environment

The WGS-MR model represented by the differential-algebraic system in **Eqs. (3)** to **(11)** and **(14)** to **(15)** was discretized using 20 finite volumes, resulting in 520 equations with 520 variables. The model was implemented in Pyomo v6.4.0 [23] and solved using Ipopt v3.13.2 [24] with linear solver ma27 [25], distributed as part of the Institute for the Design of Advanced Energy Systems Process Systems Engineering Framework (IDAES PSE) [26]. The model reliably converged in less than 0.1 CPU seconds on a laptop computer running Windows 11 with Intel® Core™ i5-8250U processor and 8GB of RAM.

Performance criteria

CO conversion is the percentage of CO in the WGS reactor feed that is reacted to produce H_2 and CO_2 as expressed below [9]:

$$\text{CO Conversion} = \left(1 - \frac{\bar{F}^{out}_{ret,CO}}{\bar{F}^{in}_{ret,CO}}\right) \times 100\%. \tag{16}$$

H_2 recovery is the percentage of available H_2 in the reactor that is recovered in the permeate outlet [9, 14]:

$$\text{H}_2\ \text{Recovery} = \left(\frac{\bar{F}^{out}_{perm,H2}}{\bar{F}^{out}_{perm,H2} + \bar{F}^{out}_{ret,H2}}\right) \times 100\%. \quad (17)$$

Model initialization procedure

In the sensitivity analysis, we solved the WGS-MR model in three steps using a multi-start initialization strategy to improve solver convergence:

Step 1: Toggle off the reaction by fixing the reaction rate variable $-r_{CO}$ to zero and deactivating **Eq. (7)**. Then, solve the resulting model. This reduces model complexity by eliminating the nonlinear reaction rate from the material balances in **Eq. (14)**.

Step 2: Activate the reaction rate expression in **Eq. (7)**, unfix and initialize the reaction rate, $-r_{CO}$, using partial pressure and temperature values from the solution from the previous step. Solve the entire model.

Step 3: Iteratively update the perturbed parameter (e.g., sweep ratio or steam/carbon ratio), defined as a mutable parameter in Pyomo, and re-solve the model for each point in the sensitivity analysis.

RESULTS

WGS-MR model reproduces the expected concentration profiles

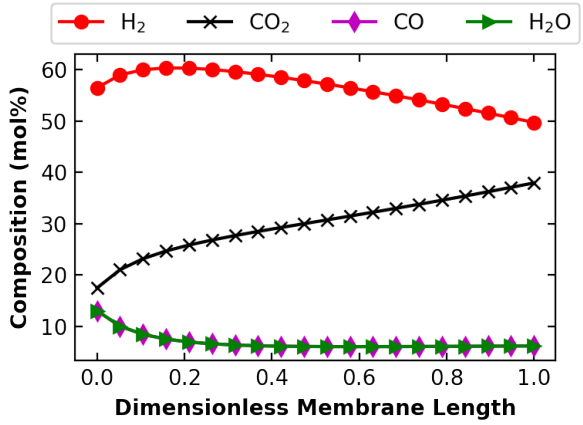

Figure 2. The retentate side concentration profiles of gas species shows that the WGS-MR model captures the relevant physics (i.e., species production/consumption by WGS reaction and H_2 depletion due to transmembrane permeation).

Figure 2 shows the retentate side composition of gas species along the dimensionless length of the reactor. As expected, the concentration of the reactants, CO and H_2O, decreases along the reactor length due to their consumption in the WGS reaction. The concentration of CO_2, on the other hand, increases along the length of the reactor. The concentration of H_2, which is the only gas permeating through the Pd-based membrane, increases and then decreases with a peak near $\bar{z} = 0.2$. The increasing H_2 concentration corresponds to the reaction-dominated regime, whereas the decreasing H_2 concentration corresponds to the transport-dominated regime. This concentration profile conforms to other WGS-MR concentration profiles reported in the literature [14, 27].

Sweep gas increases H_2 production

Using an inert sweep gas on the permeate side promotes H_2 recovery and CO conversion in the WGS-MR by increasing the driving force for H_2 permeation [9, 12]. N_2 was used as the sweep in this study. The sweep-to-feed ratio (i.e., the ratio of sweep gas flowrate to feed gas flowrate) was systematically varied to investigate the influence of sweep gas on CO conversion and H_2 recovery in the WGS-MR (**Figure 3**).

Figure 3(a) H_2 recovery: Using a N_2 sweep-to-feed ratio of 0.1 resulted in a 4% increase in H_2 recovery in the WGS-MR compared to baseline WGS-MR with no sweep. The sweep gas increases the H_2 recovery by diluting the H_2 in the permeate, which lowers its partial pressure and increases the transmembrane partial pressure difference in **Eq. (3)**, which is the driving force for H_2 flux across the membrane. For reaction temperatures of 724 K and higher, the gain in H_2 recovery plateaus at a sweep ratio of 0.1 as it approaches the theoretical maximum of 100%. Although sweep gas flow shows the potential for improving H_2 recovery in the reactor, it also dilutes the recovered H_2 which may necessitate additional purification based on the application.

Figure 3(b) CO conversion: At 724 K, a sweep-to-feed ratio of 0.5 raises CO conversion from 86% to 98%. This improvement in CO conversion is explained by the gain in H_2 recovery, which translates to increased withdrawal of a reaction product, prompting the reversible WGS reaction to be favored in the forward direction.

Generally, improved performance is observed at higher temperatures. This is the expected behavior for H_2 recovery because increasing the temperature boosts the H_2 permeance of the membrane as shown in **Eq. (4)**. However, the increased CO conversion at higher temperatures is intriguing because WGS is an exothermic reaction. We expect lower conversions at higher temperatures. We hypothesize the trends in **Figure 3(b)** are an interplay between temperature effects on the equilibrium constant and H_2 flux. Specifically, increasing the temperature enhances the flux of H_2 across the membrane, according to **Eqs. (3)** and **(4)**, shifting the equilibrium to increase CO conversion. Concurrently, the elevated temperature diminishes the equilibrium constant according to **Eq. (8)**, thereby reducing the CO conversion. **Figure 4** shows additional sensitivity analysis for varying either **(a)** reactor temperature or **(b)** membrane temperature while the other is fixed at 624 K. **Figure 4** confirms the increase in CO conversion from the increased H_2 flux outweighs the temperature shift in the reaction equilibrium.

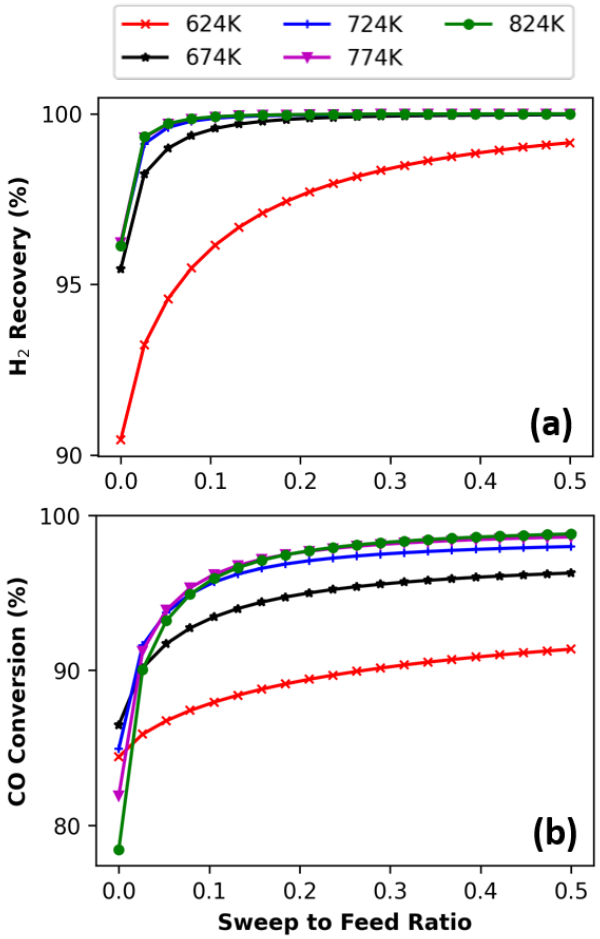

Figure 3. Increasing the sweep-to-feed ratio produces considerable gains in (a) H_2 recovery and (b) CO conversion in a WGS-MR.

CO conversion sensitive to steam/carbon ratio in a WGS-MR

Next, we vary the steam/carbon ratio in the feed (**Figure 5**). The total feed flowrate (and, by extension, the gas hourly space velocity) is fixed as reported in **Table 1**; only the relative proportions of steam and carbon in the feed changed.

Figure 5 shows that excess steam (greater than the stoichiometric ratio) promotes CO conversion in the WGS-MR. We observe that for a given feed pressure, CO conversion increases monotonically with the steam/carbon ratio up to 98 to 99% conversions at a steam/carbon ratio of 5.0. This observation is consistent with the experimental results of Bang et al. [28] for a Pd-Cu WGS-MR. Increasing the steam/carbon ratio increases reactant concentration, which triggers the forward reaction to nullify the disturbance in the equilibrium state as prescribed by La Chatelier's principle [28]. Increasing the steam/carbon ratio beyond 3.0 yields modest improvements in CO conversion as it approaches the theoretical maximum of 100%. The optimal choice of steam/carbon ratio would maximize CO conversion while constraining steam consumption in the reactor.

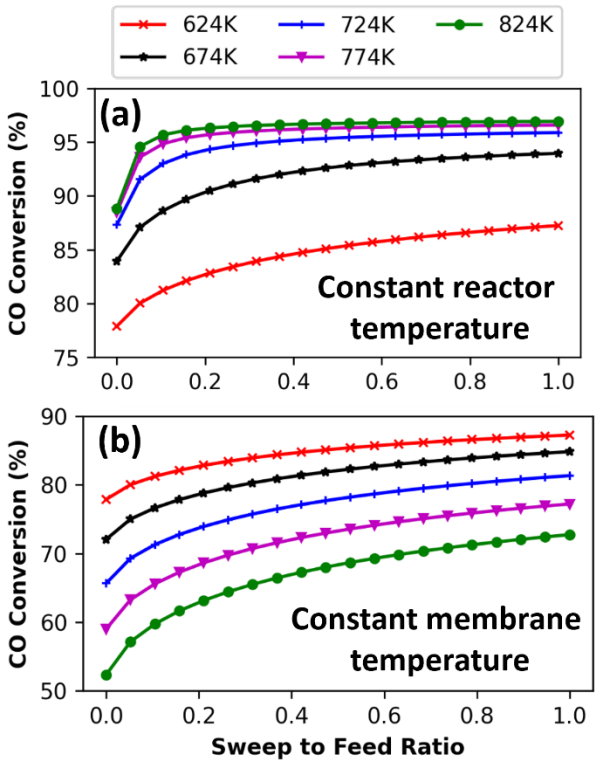

Figure 4. CO conversion as a function of sweep-to-feed ratio in a WGS-MR for two hypothetical conditions: (a) The reactor temperature is fixed at 624 K, and the membrane temperature varies. (b) The membrane temperature is fixed at 624 K and the reactor temperature varies.

Model convergence with Ipopt solver

The WGS-MR model demonstrates good solver convergence over a wide range of input parameters (e.g., feed pressures of 1 to 3 MPa, reactor temperatures of 624 to 824 K, sweep-to-feed ratios of 0 to 0.5, and steam/carbon ratios of 1 to 5). For instance, the CPU time corresponding to the sensitivity analysis results in **Figure 3** for T = 624 K is 0.26 CPU seconds for **Step 1**, 0.080 CPU seconds for **Step 2**, and 0.010 to 0.64 CPU seconds (average 0.074 CPU seconds) for **Step 3**.

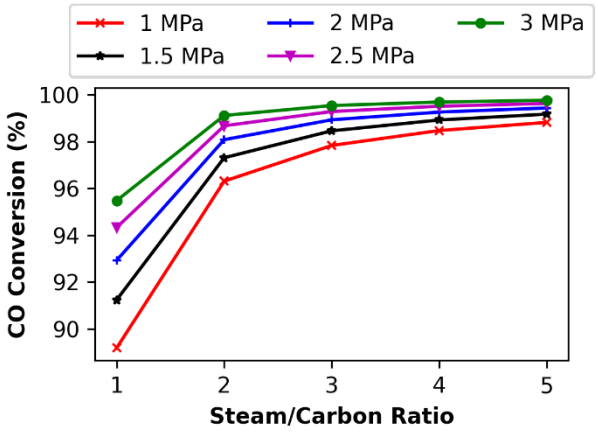

Figure 5. CO conversion in the WGS-MR increases with the steam/carbon ratio. Higher conversions are observed at higher feed pressures due to increased H_2 recovery at elevated pressures.

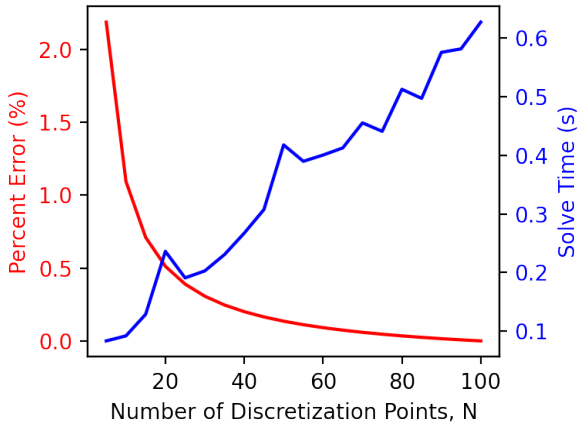

Figure 6. Sensitivity analysis quantifies the impact of the number of discretization points on the solve time and percent error. The percent error was calculated for the flowrate of H_2 in the permeate relative to the numerical solution with $N = 100$.

Table 2 compares the solver convergence performance (i.e., number of iterations and CPU seconds) of the WGS-MR model before and after rescaling the model using the initialization procedure described above. These data correspond to the sensitivity analysis in **Figure 3** and show that the scaled model converges in about 50% of the CPU seconds for the unscaled model, emphasizing the role of proper model scaling in improving numerical performance. A similar trend is observed for other temperatures and sweep-to-feed ratios in **Figure 3**, which are omitted for brevity. We found the scaled model is more robust to a naive initialization, although we recommend the procedure described above.

Table 2: Solver convergence of WGS-MR model.

		624 K		824 K	
		scaled	un-scaled	scaled	un-scaled
Sweep ratio = 0.0	# of iterations	4	4	6	7
	CPU secs	0.019	0.036	0.043	0.111
Sweep ratio = 0.2	# of iterations	4	5	5	6
	CPU secs	0.028	0.058	0.034	0.046

Figure 6 investigates the impact of the number of discretization points on the solve time and percent error. Here, percent error is defined relative to the numeric solution with $N = 100$ discretization points. As expected, the solve time increases approximately linearly with the number of disclination points, whereas the percent error decays nearly exponentially as N increases. Based on these results, we conclude that $N = 20$ is likely sufficient for process design and optimization.

CONCLUSIONS

We present an EO modeling framework for WGS-MR and propose a scaling analysis and multi-start initialization procedure that promotes solver convergence. Through sensitivity studies with this model, we show that sweep gas on the permeate side could drive up conversion to over 95% and H_2 recovery to ~99% for temperatures 674 K and above. We also show that excess steam could promote CO conversions in the WGS-MR up to a steam/carbon ratio of 3.0 for the dataset considered in this study. This EO model converges rapidly (<1 CPU sec) and serves as a tool for the design and optimization of WGS-MRs.

Ongoing work utilizes this model to optimize the technoeconomic benefits of WGS-MRs for blue H_2 production from gasified biomass. The EO modeling approach adopted in this work motivates further work into integrating the design of WGS-MR membrane modules into large-scale, EO-based flow sheets for process-wide optimization of H_2 production technologies.

ACKNOWLEDGEMENTS

This material is based upon work supported by the U.S. Department of Energy, Office of Science, Office of Basic Energy Sciences, under Award Number DE-SC0022409, with prime recipient Precision Combustion, Inc. This report was prepared as an account of work sponsored by an agency of the United States Government. Neither the United States Government nor any agency thereof, nor any of their employees, makes any warranty, express or implied, or assumes any legal

D.A. also recognizes partial support from the U.S. National Science Foundation (EEC-164772).

REFERENCES

1. Lewis, E., McNaul, S., Jamieson, M., Henriksen, M. S., Matthews, H. S., Walsh, L., Grove, J., Shultz, T., Skone, T.J. & Stevens, R. *Comparison of commercial, state-of-the-art, fossil-based hydrogen production technologies*. No. DOE/NETL-2022/3241. National Energy Technology Laboratory (NETL), Pittsburgh, PA, Morgantown, WV, and Albany, OR (United States), 2022.
2. Liguori, S., Kian, K., Buggy, N., Anzelmo, B. H., & Wilcox, J. Opportunities and challenges of low-carbon hydrogen via metallic membranes. *Progress in Energy and Combustion Science*, 80 (2020).
3. National Grid. The hydrogen colour spectrum. URL: https://www.nationalgrid.com/stories/energy-explained/hydrogen-colour-spectrum (Accessed November 13, 2023).
4. Baraj, E., Ciahotný, K., & Hlinčík, T. The water gas shift reaction: Catalysts and reaction mechanism. *Fuel*, 288 (2021), 119817.
5. Ebrahimi, P., Kumar, A., & Khraisheh, M. A review of recent advances in water-gas shift catalysis for hydrogen production. *Emergent Materials*, 3 (2020).
6. Iulianelli, A., Pirola, C., Comazzi, A., Galli, F., Manenti, F., & Basile, A. Water gas shift membrane reactors. In *Membrane reactors for energy applications and basic chemical production* (pp. 3-29) (2015). Woodhead Publishing.
7. Schwartz, J., Porter, J., Patki, N., Kelley, M., Stanislowski, J., Tolbert, S., Way, J.D. and Makuch, D. *Advanced Hydrogen Transport Membrane for Coal Gasification*. Praxair, Inc., Tonawanda, NY (United States), 2015.
8. Liu, C., Zhang, X., Zhai, J., Li, X., Guo, X., & He, G. Research progress and prospects on hydrogen separation membranes. *Clean Energy*, *7*(1), (2023).
9. Brunetti, A., Caravella, A., Barbieri, G., & Drioli, E. Simulation study of water gas shift reaction in a membrane reactor. *Journal of Membrane Science*, *306*(1-2), (2007).
10. Okazaki, J., Ikeda, T., Tanaka, D.A.P., Sato, K., Suzuki, T.M. and Mizukami, F. An investigation of thermal stability of thin palladium–silver alloy membranes for high temperature hydrogen separation. *Journal of Membrane Science*, *366*(1-2), pp.212-219, (2011).
11. Saw, S. Z., Nandong, J., & Ghosh, U. K. Optimization of steady-state and dynamic performances of water–gas shift reaction in membrane reactor. *Chemical Engineering Research and Design*, *134*, 36-51, (2018).
12. Karagöz, S., da Cruz, F. E., Tsotsis, T. T., & Manousiouthakis, V. I. Multi-scale membrane reactor (MR) modeling and simulation for the water gas shift reaction. *Chemical Engineering and Processing-Process Intensification*, *133*, 245-262, (2018).
13. Yonamine, W., Thangavel, S., Ohashi, H., & Fushimi, C. Performance analysis of a water–gas shift membrane reactor for integrated coal gasification combined cycle plant. *Energy Conversion and Management*, *174*, 552-564, (2018).
14. Gosiewski, K., & Tańczyk, M. Applicability of membrane reactor for WGS coal derived gas processing: Simulation-based analysis. *Catalysis today*, *176*(1), 373-382, (2011).
15. Giuliano, A., Poletto, M., & Barletta, D. Pure hydrogen co-production by membrane technology in an IGCC power plant with carbon capture. *International Journal of Hydrogen Energy*, *43*(41), 19279-19292, (2018).
16. Dowling, A. W., & Biegler, L. T. A framework for efficient large scale equation-oriented flowsheet optimization. *Computers & Chemical Engineering*, *72*, 3-20, (2015).
17. Ghosh, K., Vernuccio, S., & Dowling, A. W. Nonlinear reactor design optimization with embedded microkinetic model information. *Frontiers in Chemical Engineering*, *4*, (2022).
18. Biegler, Lorenz T. "New directions for nonlinear process optimization." *Current Opinion in Chemical Engineering* 21 (2018): 32-40.
19. Agi, D.T., Jones, K.D., Watson, M.J., Lynch, H.G., Dougher, M., Chen, X., Carlozo, M.N., Dowling, A.W. Computational toolkits for model-based design and optimization. *Current Opinion in Chemical Engineering*, *43:100994*, (2024).
20. Caravella, A., Hara, S., Drioli, E., & Barbieri, G. Sieverts law pressure exponent for hydrogen permeation through Pd-based membranes: Coupled influence of non-ideal diffusion and multicomponent external mass

transfer. *International journal of hydrogen energy*, *38*(36), 16229-16244, (2013).
21. Amadeo, N. E., & Laborde, M. A. Hydrogen production from the low-temperature water-gas shift reaction: Kinetics and simulation of the industrial reactor. *International journal of hydrogen energy*, *20*(12), 949-956, (1995).
22. El Hawa, H. W. A., Paglieri, S. N., Morris, C. C., Harale, A., & Way, J. D. Application of a Pd–Ru composite membrane to hydrogen production in a high temperature membrane reactor. *Separation and Purification Technology*, *147*, 388-397, (2015).
23. Bynum, M.L., Hackebeil, G.A., Hart, W.E., Laird, C.D., Nicholson, B.L., Siirola, J.D., Watson, J.P. and Woodruff, D.L. *Pyomo-optimization modeling in python* (Vol. 67). Berlin/Heidelberg, Germany: Springer, 2021.
24. Wächter, A., & Biegler, L. T. On the implementation of an interior-point filter line-search algorithm for large-scale nonlinear programming. *Mathematical programming*, *106*, 25-57, (2006).
25. HSL A Collection of Fortran Codes for Large-Scale Scientific Computation. URL: https://www.hsl.rl.ac.uk/. (Accessed November 13, 2023).
26. Lee, A., Ghouse, J.H., Eslick, J.C., Laird, C.D., Siirola, J.D., Zamarripa, M.A., Gunter, D., Shinn, J.H., Dowling, A.W., Bhattacharyya, D. and Biegler, L.T. The IDAES process modeling framework and model library—Flexibility for process simulation and optimization. *Journal of Advanced Manufacturing and Processing*, *3*(3), p.e10095, 2021.
27. Nekhamkina, O., & Sheintuch, M. Effective approximations for concentration-polarization in Pd-membrane separators. *Chemical Engineering Journal*, *260*, 835-845, (2015).
28. Bang, G., Moon, D. K., Kang, J. H., Han, Y. J., Kim, K. M., & Lee, C. H. (High-purity hydrogen production via a water-gas-shift reaction in a palladium-copper catalytic membrane reactor integrated with pressure swing adsorption. *Chemical Engineering Journal*, *411*, 128473, 2021).